PASJ: Publ. Astron. Soc. Japan **53**, 701–712, 2001 October 25

Hubble Constant at Intermediate Redshift Using the CO-Line Tully–Fisher Relation

Yoshinori TUTUI,[1, 2] Yoshiaki SOFUE,[1] Mareki HONMA,[3] Takashi ICHIKAWA,[4]
and Ken-ichi WAKAMATSU[5]
[1]*Institute of Astronomy, The University of Tokyo, Mitaka, Tokyo 181-0015*
sofue@ioa.s.u-tokyo.ac.jp
[2]*NHK, Program Production Department, Science and Environment Division, Shibuya, Tokyo 150-8001*
[3]*VERA Project Office, National Astronomical Observatory, Mitaka, Tokyo 181-8588*
[4]*Astronomical Institute, Tohoku University, Aoba, Sendai 980-8578*
[5]*Department of Technology, Gifu University, 1-1 Yanagido, Gifu 501-11*

(Received 2001 February 27; accepted 2001 August 27)

Abstract

We have determined distances and Hubble ratios for galaxies at intermediate redshifts, $cz \sim 10000$ to $35000\,\mathrm{km\,s^{-1}}$, by applying the CO-line Tully–Fisher relation to our ^{12}CO (J = 1–0)-line observations using the Nobeyama 45-m telescope, and near-IR (NIR) photometry in the J- and H-bands using the 1.88-m telescope at Okayama Astrophysical Observatory. By averaging the Hubble ratios from the J-band result, we obtained a Hubble constant of $H_0 = 60 \pm 10\,\mathrm{km\,s^{-1}\,Mpc^{-1}}$. We argue that the CO line–NIR Tully–Fisher relation can be a complimentary method to the other methods for measuring the distances of galaxies at intermediate and high redshifts.

Key words: cosmology: Hubble constant — galaxies: distances and redshifts — ISM: CO line

1. Introduction

The H I-line Tully–Fisher relation (TFR) has been established as one of the most reliable methods to determine the distances of galaxies, and has been successfully applied for detemining the Hubble constant (Tully, Fisher 1977; Aaronson et al. 1980; Giovanelli et al. 1995; Giovanelli, Haynes 1985; Haynes, Giovanelli 1986). The use of the CO lines has been proposed as a complimentary method to H I (Sofue 1992; Dickey, Kazès 1992; Sofue et al. 1996). Compatibility between the CO and H I line-widths has been confirmed for nearby galaxy samples (Schöniger, Sofue 1994, 1997; Lavezzi, Dickey 1998; Tutui, Sofue 1999; Tutui et al. 2000).

The CO-line TFR has some advantages, particluarly at higher redshifts. Since the molecular-gas distribution in a galaxy is tightly correlated with the luminousity distribution, the CO-line width can be properly compared with the photometric luminosity. CO gas distributions are less affected by galaxy interactions and intracluster medium compared to H I, and the CO gas is not particularly deficient, even in cluster-center galaxies (Kenney, Young 1988; Casoli et al. 1991), which enables us to apply the TFR to rich-cluster galaxies. These properties will be helpful to apply the TFR to high redshifts, at which the fraction of interacting and merging galaxies is supposed to be greater than at low redshifts. Since high-redshift galaxies are supposed to be more dusty than nearby galaxies, near-IR photometry would be more appropriate than optical. Thus, the CO–NIR TFR would be a promising method to determine the distances of intermediate and high-redshift galaxies, and particularly for cluster galaxies at high redshifts.

In this paper we report on the result of an extensive CO TFR program using the Nobeyama 45-m mm-wave telescope, and NIR photometry using a 1.88-m telescope at Okayama Astrophysical Observatory. The program has been performed as a pilot program to promote a more sensitive, higher resolution CO–NIR TFR project using the Nobeyama mm-wave array, and an advanced array linked to the 45-m telescope. We obviously aim at obtaining basic data for higher-transition CO line TFR using the Atacama large mm-wave and sub-mm-wave array (ALMA) in the near future.

2. Observations

2.1. Sample Selection

We selected isolated galaxies of normal morphology as a sample according to the following criteria:

(1) The redshift range of the sample was taken to be cz = 10000–20000 km s^{-1} in 1994/1995 observations, cz = 20000–30000 km s^{-1} in 1995/1996, and cz = 30000–50000 km s^{-1} in 1996/1997 observations. The CO data are published in Tutui et al. (2000) for a discussion of CO and the infrared properties of non-interacting IRAS galaxies at intermediate redshifts.

(2) We selected relatively strong FIR-emission sources at 60 μm and 100 μm, typically greater than 1 Jy, which are supposed to be bright in the CO line. Such FIR luminous galaxies are supposed to be affetected by efficient star formation. For this reason, we use NIR luminosities, instead of blue luminosities, which may be strongly affected by the star formation. However, we also emphasize that the TFR applies to IRAS galaxies with much higher FIR luminosities (van Driel et al. 1995).

(3) In order to minimize the effect of galaxy–galaxy interaction, we selected galaxies with normal morphologies using DSS (STScI Digitized Sky Survey) images. Strongly interacting galaxies and mergers were not included. They are not likely

to be starburst galaxies.

(4) Since the half-power beam width (HPBW) of the NRO 45-m telescope was 15″, galaxies whose position error listed in the NASA Extragalactic Database (NED) is less than 10″ were selected. We also cross-checked the position using the DSS images. The 15″-beam corresponds to $\sim 30\,\mathrm{kpc}$ at $z \sim 0.1$. Hence, we may safely assume that most of CO-emitting disks are covered by the beam.

(5) Since the line-widths of the objects were expected to be about 200 to $500\,\mathrm{km\,s^{-1}}$, we selected galaxies with a recession velocity accuracy better than $100\,\mathrm{km\,s^{-1}}$ in order to fit a band width (250 MHz) corresponding to $650(1+z)\,\mathrm{km\,s^{-1}}$. The recession velocity was taken from the IRAS redshift surveys by Strauss et al. (1992) and Fisher et al. (1995).

The CO and far-infrared properties of individual objects are described in detail in Tutui et al. (2000). The objects were selected based on their isolated and normal morphology. This is in contrast to the existing CO observations from the literature, which are mostly for interacting/merging systems. Using these new data, Tutui et al. (2000) have discussed the molecular-gas and dust properties of late-type galaxies at intermediate redshifts. We stress that our sample presents the deepest CO observations of non-intreacting/non-merging IRAS galaxies at intermediate redshifts. The galaxies are shown to have a normal star-formation efficiency, normal color–color diagrams, and not particularly strong nuclear activity. However, they show a smaller gas-to-dust ratio than the usual (brighter) IRAS galaxies. Nevertheless, our IRAS selected sample could contain starburst galaxies, which would have higher luminosities compared to those of normal galaxies. However, we note that van Driel et al. (1995) have examined the TF relation for IRAS selected galaxies, and found little difference from the TF relation of normal galaxies. Since galaxies rich in CO are often rich in H I, one might wonder how many galaxies in this sample are detected in H I. However, in so far as we have checked NED, there have been no H I detection.

2.2. *CO-Line Observations*

The observataions of the ^{12}CO (J = 1–0) line were carried out using the 45-m telescope at the Nobeyama Radio Observatory as a long-term project at NRO. The observations were carried out in 1994 January/December, 1995 January/March/December, 1996 January/February/December, and 1997 January. The HPBW of the NRO 45-m telescope was 15″ at the frequency of ^{12}CO (J = 1–0) line, and the aperture and main-beam efficiencies were $\eta_{\mathrm{a}} = 0.35$ and $\eta_{\mathrm{mb}} = 0.50$, respectively. As the receiver frontends, we used cooled SIS (superconductor–insulator–superconductor) receivers. The receiver backends were 2048-channel wide-band acousto-optical spectrometers (AOS) with a band width of 250 MHz, which corresponds to a velocity coverage of $650(1+z)\,\mathrm{km\,s^{-1}}$, or 650 ($z = 0$) to $780\,\mathrm{km\,s^{-1}}$ ($z = 0.2$).

The center frequency was set at the 1024-th channel, which corresponded to $115.271204(1+z)^{-1}$ GHz for each galaxy. The system noise temperature was 300–800 K in the single side band at the observing frequencies. A calibration of the line intensity was made using an absorbing chopper in front of the receiver, yielding the antenna temperature (T_{A}^{*}), corrected for both atmospheric and antenna ohmic losses. The intensity scale of T_{A}^{*} was converted to the main-beam brightness temperature by $T_{\mathrm{mb}} = T_{\mathrm{A}}^{*}/\eta_{\mathrm{mb}}$. Subtraction of the sky emission was performed by on–off position switching; the offset of the off-position was 5′ far from the on-position. Antenna pointing of the NRO 45-m telescope was done by observing nearby SiO maser sources at 43 GHz every 60 to 90 min, where the two receiveres (115 and 43 GHz) were well aligned for this purpose. The pointing accuracy was better than ±4″ during the observations. The total observation time for the on/off position integrations and pointing was about 2 to 9 hr for individual galaxies, and the on-source integration time for each galaxy was 1 to 3 hr.

After flagging bad spectra, subtraction of the baseline was performed by applying the standard procedure of linear-baseline fitting at both edges of individual spectra. Adjacent channels were binned to a velocity resolution of $10\,\mathrm{km\,s^{-1}}$. The rms noise of the resultant spectra at a velocity resolution of $10\,\mathrm{km\,s^{-1}}$ was 2–5 mK in T_{A}^{*}.

2.3. *CO-Line Profiles and Line-Widths*

We observed 51 galaxies at intermediate redshifts of $cz \sim$ 10000–$50000\,\mathrm{km\,s^{-1}}$ and obtained CO-line profiles of 17 galaxies, as listed in table 1. The observed CO-line profiles are shown in figure 1. These galaxies are the deepest CO-line sample of IRAS galaxies with non-interacting, normal morphology (Tutui et al. 2000). The detection probability is not high compared to that of the LIR galaxies, because the sample consists of very distant galaxies of normal morphology. The CO luminosities for an assumed Hubble constant of about $60\,\mathrm{km\,s^{-1}\,Mpc^{-1}}$, as will be obtained in the later section, are comparable to those of high-mass spirals; and the estimated molecular hydrogen mass of the galaxies is of the order of $10^9\,M_{\odot}$ for a conversion factor of $2 \times 10^{20}\,\mathrm{H_2\,[K\,km\,s^{-1}]^{-1}}$.

We determined the CO line-widths at the 20% level of the peak intensity. Although the line profiles are noisy with typical S/N ratios of about 10, the line-widths are determined within an error of $\Delta W \sim 10$ to $20\,\mathrm{km\,s^{-1}}$. Since the expected line shapes from rotating disks are not straightforward, like Gaussian, no automatic algorithm has been applied. Instead, we judged the lines by eyes, and the errors were taken to be the uncertainty in the edge channels of the lines. One channel after smoothing, as in the figure, is $10\,\mathrm{km\,s^{-1}}$. Three galaxies (IRAS 02411+0354, IRAS 07243+1215, and IRAS 14210+4829) are found to be too crude for TF analyses. The CO line-width is defined as

$$W_{\mathrm{obs}} \equiv c\,\frac{\Delta\nu}{\nu_{\mathrm{obs}}}, \tag{1}$$

where $\Delta\nu$ at the line-width at the observed frequency and ν_{obs} is the observed center frequency of the spectrometer. The results of the observations are listed in table 2.

2.4. *H- and J-Band Photometry*

Besides the CO-line observations, we obtained near-IR (NIR) photometry in the J- and H-bands (Aaronson et al. 1980). In these NIR bands, the interstellar extinction in our Galaxy and target galaxies is greatly reduced compared to that of the B-band. This is particularly helpful for the present galaxies, which were selected from IRAS bright galaxies for CO-line detections. The NIR luminosity of IRAS Minisurvey galaxies

Table 1. Galaxies detected in the CO-line using the NRO 45-m telescope.

Galaxy (IRAS ID)	RA_{1950}	Dec_{1950}	cz	z	D_{cz}	J-band size
	h m s	° ′ ″	$km\,s^{-1}$		Mpc	″×″
PG 0157+001 (01572+0009)	01 57 16.3	+00 09 09	48869	0.16301	677	24 × 15
IRAS 02185+0642	02 18 40.3	+06 43 03	29347	0.09789	401	19 × 17
IRAS 02411+0354†	02 41 09.3	+03 53 56	43050	0.14360	594	
IRAS 07243+1215†	07 24 20.6	+12 15 09	28204	0.09408	385	
I Zw 23 (09559+5229)	09 56 01.0	+52 29 48	12224	0.04077	165	31 × 25
CGCG 1113.7+2936 (11137+2935)	11 13 47.1	+29 35 58	13880	0.04630	187	50 × 31
IC 2846 (11254+1126)	11 25 24.8	+11 26 01	12294	0.04101	166	46 × 27
IRAS 14060+2919	14 06 04.9	+29 18 59	35060	0.11695	481	17 × 11
CGCG 1417.2+4759 (14172+4758)	14 17 14.8	+47 59 00	21465	0.07160	291	25 × 21
IRAS 14210+4829†	14 21 06.2	+48 29 59	22690	0.07569	308	
CGCG 1448.9+1654 (14488+1654)	14 48 54.5	+16 54 02	13700	0.04570	185	23 × 19
NGC 6007 (15510+1206)	15 51 01.6	+12 06 27	10547	0.03518	142	85 × 43
IRAS 16533+6216	16 53 19.8	+62 16 36	31808	0.10610	435	13 × 12
PGC 60451 (17300+2009)	17 30 00.6	+20 09 49	14989	0.05000	202	
IRAS 17517+6422	17 51 45.0	+64 22 14	26151	0.08723	356	
IRAS 23389+0300	23 38 56.9	+03 00 48	43470	0.14500	600	
IRAS 23420+2227	23 42 00.6	+22 27 50	26022	0.08680	354	15 × 10

Col. (1): Galaxy name. A dagger denotes a galaxy of marginal detection. Alias of the galaxy name as the IRAS catalog name is in the brackets. Col. (2) and (3): Coordinates in B1950. Col. (4): Heliocentric velocity. Col. (5): Heliocentric redshift from Fisher et al. (1995). Col. (6): Distance derived from the redshift, assuming $H_0 = 75\,km\,s^{-1}\,Mpc^{-1}$ and $q_0 = 0.5$. Col. (7): J-band angular size in arcsec for galaxies observed in the present photometry imaging.

has been shown not to be significantly enhanced compared to the *RSA* sample (van Driel et al. 1995).

Surface photometry observations were made in 1999 January in the J- (1.25 μm) and H-band (1.65 μm) using OASIS, a NIR spectroscopic and imaging camera attached to the Cassegrain focus of the 1.88-m reflector at the Okayama Astrophysical Observatory. The detector was a NICMOS-3, which consisted of 256 × 256 pixels. The seeing size was 1.″7–2.″1 (FWHM), and the sky level was typically 16 mag in the J-band and 14 mag in the H-band. One pixel corresponded to 0.″97, and the field-of-view was approximately 4′. The exposure time per one frame was 30–80 s for the J-band and 10–30 s for the H-band, and the total integration time was about 20 min for each band per one galaxy. A flux calibration was performed using the standard stars in the J- and H-bands presented by Hunt et al. (1998) before and after each observation of galaxies. Standard data processing (dark current subtraction, image shifting/combining and flat fielding) were performed with the IRAF software package, and subsequent surface photometry and image processing (e.g. sky subtraction and flux measurement) were performed with the SPIRAL package developed at the Kiso Observatory and incorporated into the IRAF system (Hamabe, Ichikawa 1992). Figure 2 shows the obtained J-band images.

We obtained J- and H-band photometric observations for 12 galaxies out of the 17 CO-detected galaxies, and measured the total magnitude. However, IRAS 17517+6422 was found to be an interacting galaxy; we did not include this galaxy in our TF analysis. Also, PG 0157+001 was found to be a quasar, and was not included. Hence, the TF analysis was applied to the remaining 10 galaxies, as listed in table 4.

We measured the integrated magnitude of the galaxies within a circular annulus outward from the galaxy center at 1 pixel intervals. We define the total magnitude as the converged value of the growth curve. The thus-defined total magnitude has an error as large as 0.1 mag, since the galaxy morphology is not well determined (de Vaucouleurs et al. 1991).

The following corrections were applied to the observed total magnitude, m_T to obtain a corrected total magnitude m_T^0:

$$m_T^0 = m_T - A_i - A_G - K(z), . \quad (2)$$

where A_i is the internal extinction within the target galaxy, which was calculated from the B-band value taken from RC3 (de Vaucouleurs et al. 1991; Watanabe et al. 1998) using the formula $A_i^J = 0.21A_i^B$ and $A_i^H = 0.13A_i^B$ (Rieke, Lebofsky 1985). The Galactic extinction, A_G, was taken from Berstein and Heiles (1982). The K-correction, a correction for a redshifted wavelength of observed passbands, was estimated by assuming the spectral model of Poggianti (1997) for an Sc galaxy. The corrected total magnitude, m_T^0, in equation (2) was further corrected for the evolution, E-correction, adopted from Poggianti (1997). We defined the total magnitude corrected for K and E-corrections, m_T^1, as

$$m_T^1 = m_T - A_i - A_G - K(z) - E(z). \quad (3)$$

The error of the corrected magnitudes is assumed to be the same as that of the observed values of m_T, 0.1 mag. The values of these corrections and the corrected magnitudes are also listed in table 3. The error of the thus-calculated corrected magnitudes is assumed to be the same as that (0.1 mag) for the observed values of m_T.

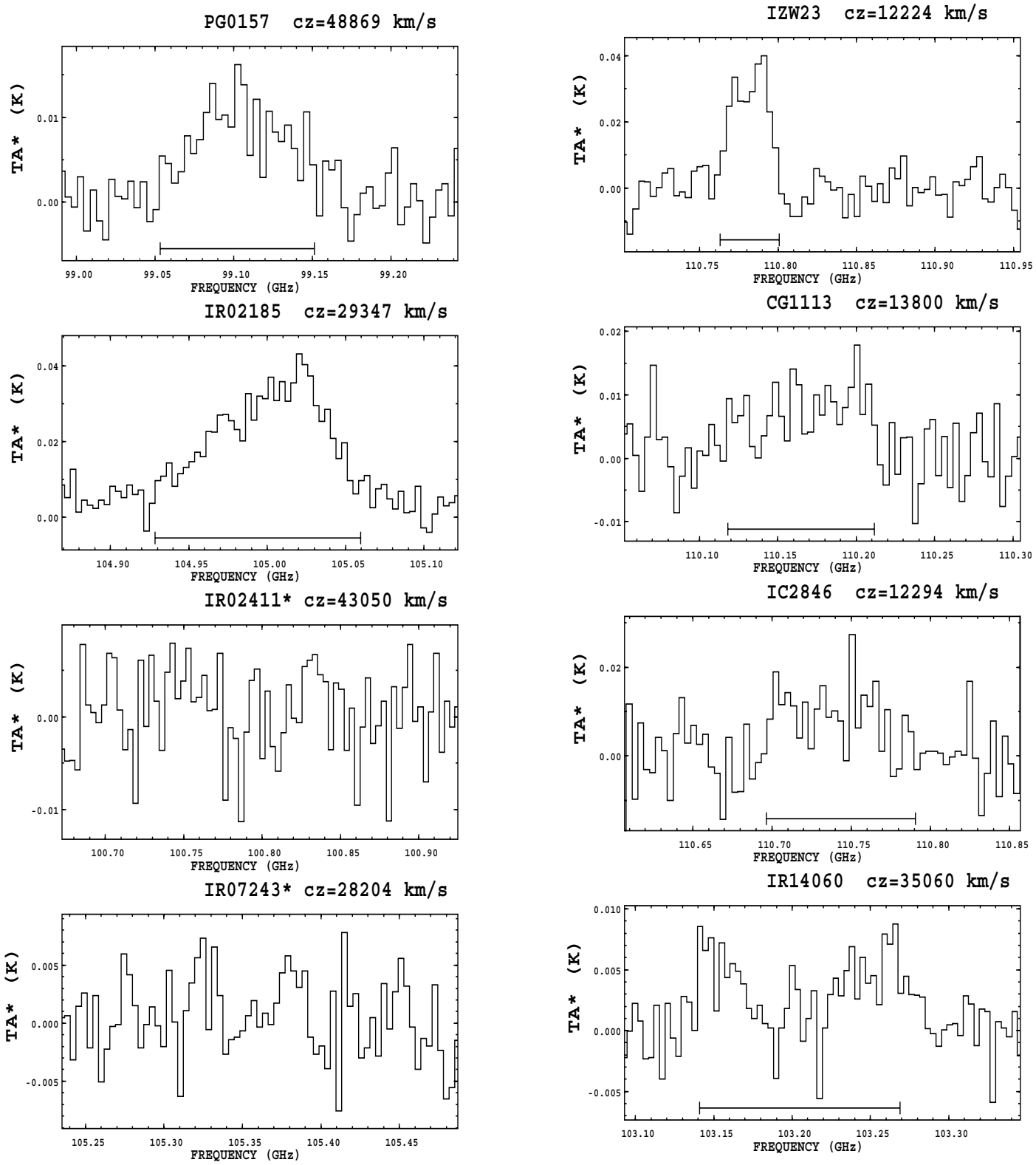

Fig. 1. CO line profles for 17 galaxies. The horizontal bars indicate the measured line-widths. Galaxies with asterisks are for marginal and non-detection, which are not included in the distance estimation.

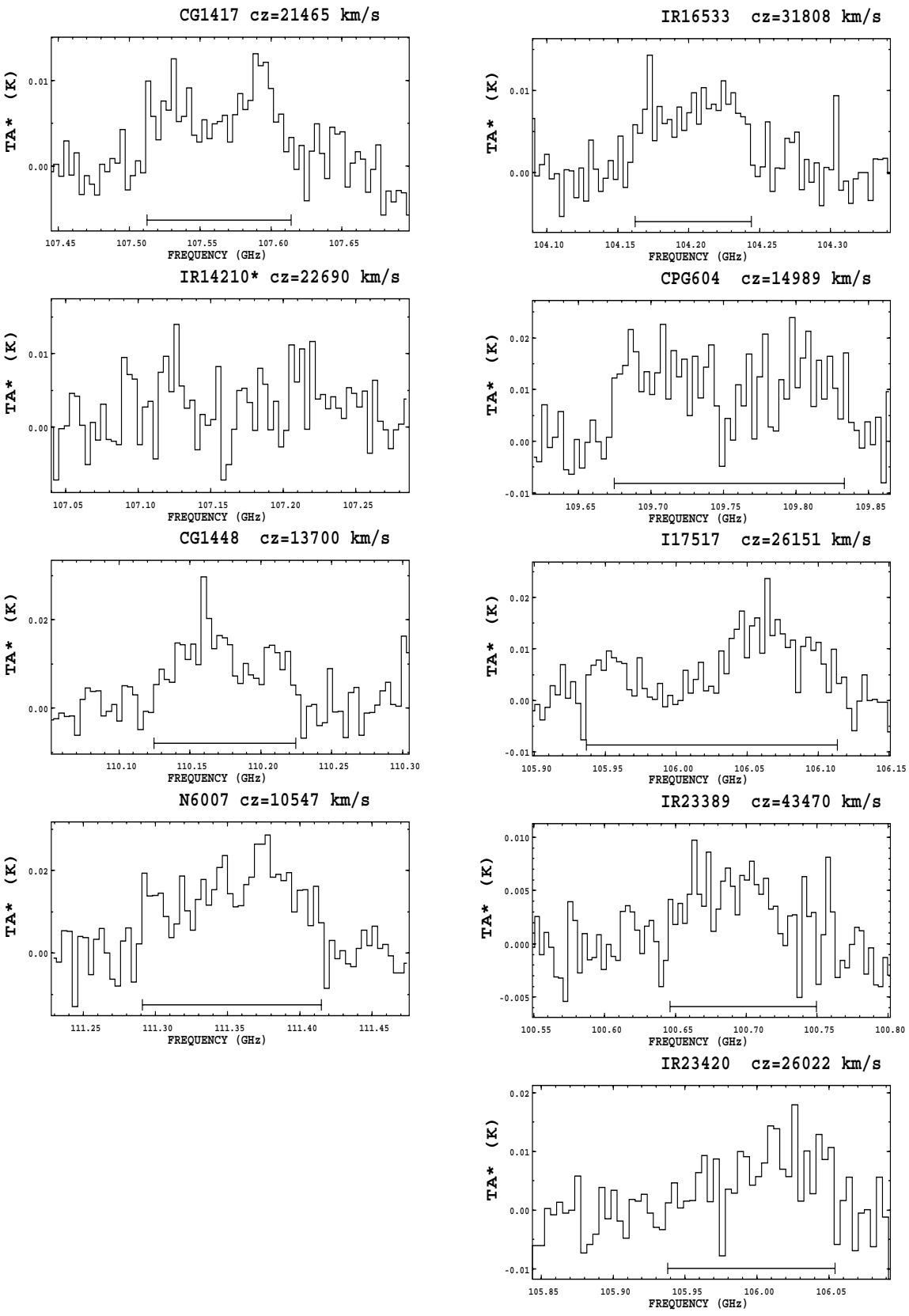

Fig. 1. (Continued)

Table 2. CO-line observation results using the NRO 45-m telescope.

Galaxy	cz	$t_{\rm int}$	r.m.s.	$W_{\rm obs}$	$T_{\rm A}^*$	$I_{\rm CO}$	
	km s^{-1}	min	mK	km s^{-1}	mK	K km s^{-1}	
PG 0157+001	48869	90	2	300 ± 15	15	5.11	(0.22)
IRAS 02185+0642	29347	90	4	356 ± 15	40	13.05	(0.48)
IRAS 02411+0354†	43050	60	5	···	8	1.90	(0.66)
IRAS 07243+1215†	28204	90	3	···	6	1.79	(0.28)
IZw 23	12224	60	4	104 ± 5	39	4.82	(0.26)
CGCG 1113.7+2936	13880	60	5	248 ± 20	14	4.33	(0.55)
IC 2846	12294	30	4	360 ± 20	19	4.78	(0.48)
IRAS 14060+2919	35060	120	3	376 ± 20	8	1.91	(0.37)
CGCG 1417.2+4759	21465	180	3	293 ± 15	13	4.66	(0.32)
IRAS 14210+4829†	22690	60	4	···	11	3.08	(0.54)
CGCG 1448.9+1654	13700	60	4	282 ± 10	28	7.03	(0.42)
NGC 6007	10547	60	7	347 ± 10	28	11.24	(0.82)
IRAS 16533+6216	31808	90	3	217 ± 10	10	3.54	(0.28)
PGC 60451	14989	60	7	459 ± 15	20	10.35	(0.95)
IRAS 17517+6422	26151	90	5	480 ± 20	19	4.00	(0.69)
IRAS 23389+0300	43470	180	3	272 ± 20	8	3.92	(0.31)
IRAS 23420+2227	26022	60	7	308 ± 20	15	4.80	(0.49)

Col. (1): Galaxy name. A dagger denotes a galaxy of marginal detection. Col. (2): Redshift in cz. Col. (3): Integration time of on-source in min. Col. (4): Root-mean-square of antenna temperature after binning of 10 km s^{-1} in emission-free region of the spectrum. Col. (5): Observed CO line-width defined as the full width at 20% of the maximum intensity. Col. (6): Antenna temperature at the peak level intensity. Col. (7): Integrated intensity corrected for the main beam efficiency. Col. (8): Uncertainty of 1σ in the integrated intensity.

3. Determination of the Hubble Constant

3.1. Inclination Correction

Since B-band images would be affected by recent star formation, which disturbs the isophote in bluer bands, we used R-band images taken from the STScI Digitized Sky Survey for determining the inclination angle, using the conventional formula given by Hubble (1926),

$$\cos^2 i = \frac{(b/a)^2 - q_0^2}{1 - q_0^2}, \tag{4}$$

where b/a is the minor-to-major axial ratio and q_0 is an intrinsic axial ratio fixed to 0.2. The disk images of the sample galaxies in the J- and H-bands are too faint against the high sky background to fit the major and minor axes. Therefore, we adopted the deeper optical R-band images for obtaining the inclination.

3.2. Conversion of CO to H I Line-Widths

The inclination-corrected CO-line velocity-width is then calculated as

$$W_{\rm CO}^{\rm c} = \frac{W_{\rm obs}}{\sin i}, \tag{5}$$

where i is the inclination angle, and suffix c denotes the corrected line-width. Tutui and Sofue (1999) and Tutui (1999) showed that the CO line-width is not entirely identical with the H I line-width,

$$W_{\rm HI}^{\rm c} = 0.76 W_{\rm CO}^{\rm c} + 83.8. \tag{6}$$

The H I line-width is slightly larger than the CO width for slowly rotating galaxies, and vice versa for rapidly rotating galaxies. This is caused by a different gas distribution in a galaxy and by the velocity-dependence on the shape of the rotation curve. These corrected line-widths are listed in table 4. Note that, according to this equation, $W_{\rm HI}^{\rm c}$ and $W_{\rm CO}^{\rm c}$ coincide within the error for galaxies with typical line-widths of around 350 km s^{-1}.

3.3. Adopted Tully–Fisher Relations

We then applied the H I Tully–Fisher relation in J- and H-bands derived by Watanabe et al. (2001) for the thus-corrected values of $W_{\rm HI}^{\rm c}$. Watanabe et al. (2001) calibrated the TF relations using the local calibrators with the Cepheid distances observed by HST, where the zero-point calibrations were performed for the calibrators observed with the Kiso Observatory 105-cm Schmidt telescope. We obtained the total magnitude, the inclination, the extinction correction, and the line-width in the same way as those of the calibrators:

$$M_{J_{\rm T}} = -8.48(\pm 0.85)\,(\log W_{\rm HI}^{\rm c} - 2.5) - 22.13(\pm 0.39) \quad (\sigma = 0.30) \tag{7}$$

and

$$M_{H_{\rm T}} = -7.54(\pm 0.76)\,(\log W_{\rm HI}^{\rm c} - 2.5) - 22.95(\pm 0.35) \quad (\sigma = 0.28). \tag{8}$$

3.4. Determination of Hubble Constant

The luminosity distance derived from the TFR is given by the distance modulus, $m - M$, as

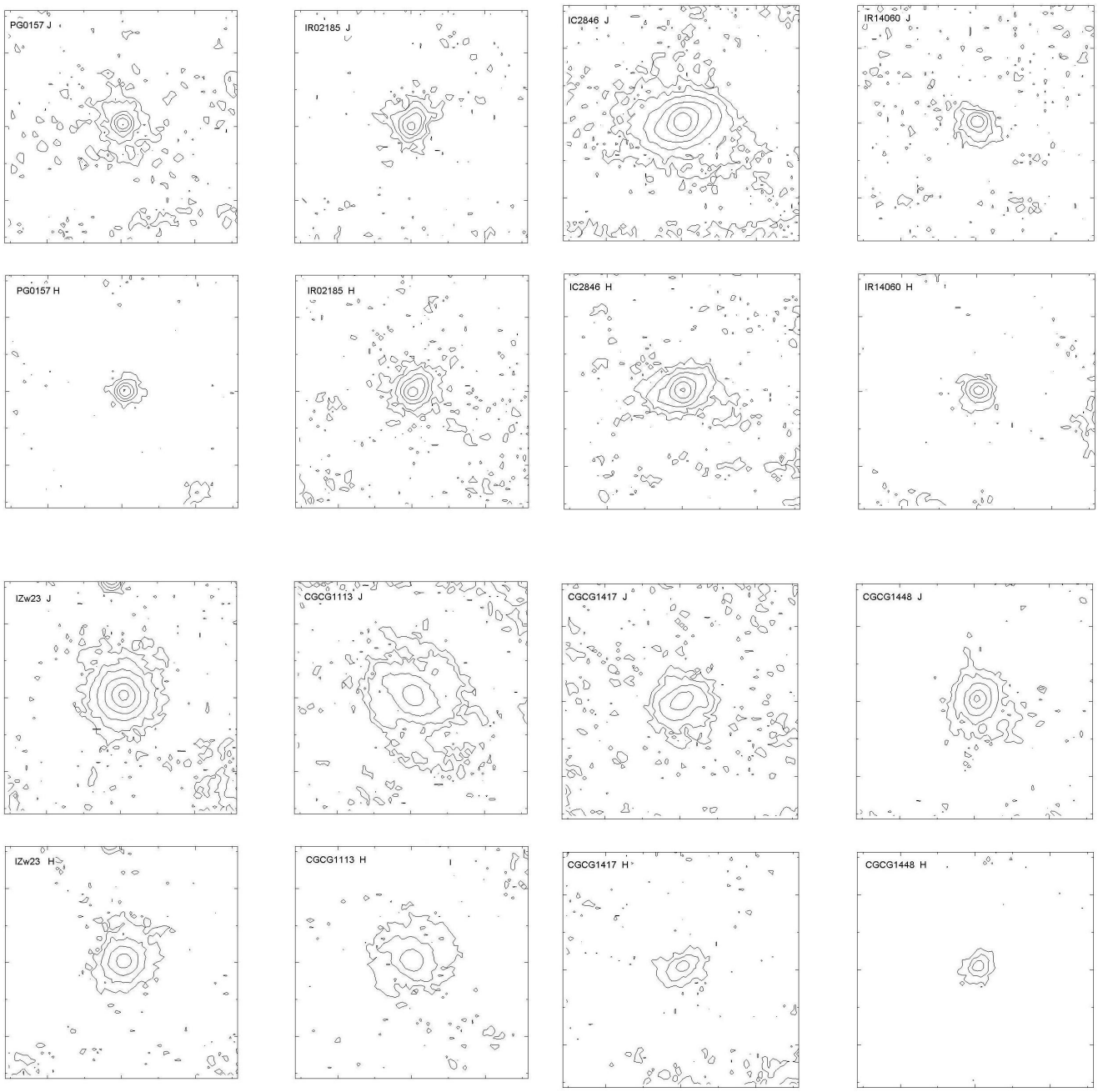

Fig. 2. J-, H- and K-band images of the measured galaxies. The image sizes are $1' \times 1'$, except for NGC 6007 of $2' \times 2'$. The faintest isophote is 22 mag arcsec^{-2} for the J-band and 20 mag arcsec^{-2} for the H-band. The contour interval is 1 mag arcsec^{-2}. Top is to the north, and left is to the east.

$$\log D_L = -5 + \frac{1}{5}(m - M) \quad \text{(Mpc)}, \tag{9}$$

where m is apparent total magnitude. The luminosity distance is related to the Hubble constant as

$$D_L = \frac{c}{H_0 q_0^2}\left\{q_0 z + (q_0 - 1)(\sqrt{2q_0 z + 1} - 1)\right\}, \tag{10}$$

where q_0 is the deceleration parameter; we use $q_0 = 0.5$. Then, the Hubble ratio is written as

$$H_0 = \frac{2c}{D_L}(z + 1 - \sqrt{z + 1}). \tag{11}$$

For a small redshift, $z \ll 1$, this relation reduces, of course, to $H_0 = cz/D_L$. The obtained Hubble ratios for all sample galaxies are listed in table 5.

The distances and Hubble ratios derived from the Tully–Fisher relations are listed in table 5, and the J- and H-band results after K-correcitons are plotted in figure 3. We then calculated the mean Hubble constant in the observed redshift range by weight-averaging the individual values, the results of which are listed in table 6. Thereby, values exceeding the 3σ dispersion of the plots were excluded. Namely, two galaxies, IZw 23 and CGCG 1113.7+2936, as well as the quasar PG 0157 were

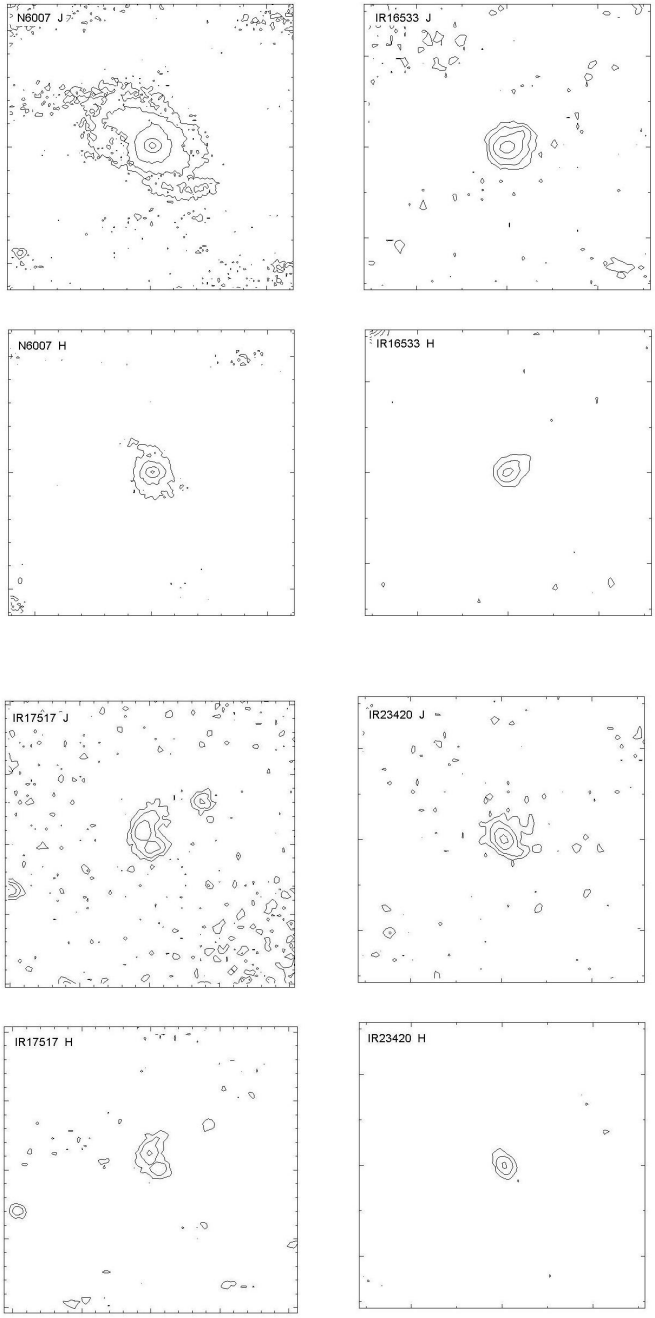

Fig. 2. (Continued)

excluded from the sample. Note that the plots in figure 3 are more scattered for lower redshift galaxies, for which the beam size (15″) could not cover the whole CO emitting regions.

The weighted mean value of the Hubble ratios from the J-band results after a K-correction was obtained to be $H_0 = 60 \pm 10\,\mathrm{km\,s^{-1}\,Mpc^{-1}}$. The H-band result leads to $H_0 = 53 \pm 13\,\mathrm{km\,s^{-1}\,Mpc^{-1}}$. The Hubble ratios for the J- and H-band are almost equal for some galaxies, confirming that the uncertainty in the surface photometry in the J- and H-band is small. The K- and E-corrected Hubble constant was determined to be $H_0 = 58 \pm 10\,\mathrm{km\,s^{-1}\,Mpc^{-1}}$ in the J-band and $H_0 = 52 \pm 12\,\mathrm{km\,s^{-1}\,Mpc^{-1}}$ in the H-band, which are only 3% smaller than the value after the K-correction alone.

3.5. Errors

Given a TF relation, the error in the absolute magnitude, ΔM, arises from the errors in the CO line-width, $\Delta W_{\rm obs}$, inclination, Δi, and redshift, Δz, which propagate to each other as follows:

$$\Delta M = \sqrt{\left(\frac{\Delta W_{\rm obs}}{W_{\rm obs}}\right)^2 + \left(\frac{\Delta i}{\tan i}\right)^2 + \left(\frac{\Delta z}{1+z}\right)^2} \cdot |A| \log e, \quad (12)$$

where A is the slope of the TFR. The error in the luminosity distance is thus related to the error in the absolute magnitude, as above, and the error in the apparent magnitude measurement:

$$\frac{\Delta D_L}{D_L} = \frac{\Delta(m-M)}{5\log e} = \frac{1}{5\log e}\sqrt{\Delta m^2 + \Delta M^2} \quad (13)$$

and

$$\frac{\Delta D_L}{D_L} = \frac{1}{5\log e} \times \sqrt{\Delta m^2 + \left\{\left(\frac{\Delta W_{\rm obs}}{W_{\rm obs}}\right)^2 + \left(\frac{\Delta i}{\tan i}\right)^2 + \left(\frac{\Delta z}{1+z}\right)^2\right\}} \times \sqrt{|A|^2 (\log e)^2}. \quad (14)$$

For a small redshift, the error in the Hubble ratio is written as

$$\frac{\Delta H_0}{H_0} = \sqrt{\left(\frac{\Delta z}{z}\right)^2 + \left(\frac{\Delta D_L}{D_L}\right)^2}. \quad (15)$$

The contribution of the errors in the total magnitude, Δm, and redshift, Δz, to the error of the distance estimation is much smaller than that of the errors of line-width, $\Delta W_{\rm obs}$, and inclination, Δi, which was measured to be about 4.°8 for all galaxies. Therefore, the first and 4th terms in the square root of equation (14) are negligible compared to the other terms. The error in the resultant Hubble ratio increases with decreasing line-width. The beam-size effect is crucial for lower redshift galaxies. It may happen that the telescope beam cannot cover the entire CO extent for large angular diameter galaxies. The telescope beam (15″) corresponds to 36 kpc for a galaxy at $cz = 30000\,\mathrm{km\,s^{-1}}$ for our resulting Hubble constant of about $60\,\mathrm{km\,s^{-1}\,Mpc^{-1}}$. This diameter covers a substantial portion of the interstellar gas disks, and the detected CO line well represents the maximum velocity-width. However, for lower redshift galaxies than $15000\,\mathrm{km\,s^{-1}}$, for example, the beam might not cover the entire disk, which may result in an underestimation of the line-width and, therefore, an underestimation of the Hubble ratio. In fact, the scatter of the plot in figure 3 increases with decreasing redshift, implying that the beam effect for low-redshift galaxies would not be negligible. The result would therefore be more reliable for galaxies at $cz > 20000\,\mathrm{km\,s^{-1}}$ in the present case for the 45-m telescope.

4. Discussion

Peculiar velocities of galaxies, either individual or due to large-scale structures in clusters and networks, contribute significantly to the scatter in the Hubble ratios. Therefore, in order

Table 3. Total magnitude and correction for magnitude.

Galaxy	$m_{\rm T}$ mag	A_i mag	$A_{\rm G}$ mag	K mag	E mag	$m^0_{\rm T}$ mag	$m^1_{\rm T}$ mag
(J-band)							
PG 0157+001	14.23	0.02	0.04	−0.09	−0.17	14.26	14.43
IRAS 02185+0642	14.37	0.02	0.04	−0.06	−0.10	14.37	14.47
I Zw 23	12.77	0.02	0.04	−0.03	−0.05	12.74	12.79
CGCG 1113.7+2936	13.41	0.05	0.03	−0.04	−0.05	13.37	13.42
IC 2846	12.26	0.03	0.04	−0.03	−0.05	12.21	12.26
IRAS 14060+2919	15.10	0.03	0.03	−0.07	−0.12	15.11	15.23
CGCG 1417.2+4759	13.89	0.02	0.04	−0.05	−0.08	13.88	13.96
CGCG 1448.9+1654	14.12	0.02	0.04	−0.03	−0.05	14.09	14.15
NGC 6007	12.66	0.03	0.05	−0.03	−0.05	12.61	12.66
IRAS 16533+6216	15.16	0.02	0.05	−0.07	−0.14	15.15	15.29
IRAS 23420+2227	15.64	0.03	0.04	−0.06	−0.10	15.63	15.73
(H-band)							
PG 0157+001	13.32	0.01	0.02	−0.08	−0.16	13.37	13.53
IRAS 02185+0642	13.18	0.02	0.03	−0.04	−0.10	13.17	13.27
I Zw 23	12.26	0.01	0.03	−0.02	−0.04	12.24	12.28
CGCG 1113.7+2936	12.34	0.03	0.02	−0.02	−0.05	12.31	12.36
IC 2846	11.49	0.02	0.02	−0.02	−0.04	11.47	11.51
IRAS 14060+2919	14.57	0.02	0.02	−0.05	−0.12	14.58	14.70
CGCG 1417.2+4759	13.32	0.01	0.02	−0.03	−0.08	13.31	13.39
CGCG 1448.9+1654	13.98	0.02	0.02	−0.02	−0.05	13.96	14.01
NGC 6007	12.37	0.02	0.03	−0.01	−0.04	12.33	12.37
IRAS 16533+6216	14.52	0.01	0.03	−0.04	−0.11	14.52	14.63
IRAS 23420+2227	14.91	0.02	0.02	−0.04	−0.09	14.90	14.99

Col. (1): Galaxy name. Col. (2): Observed total magnitude. Col. (3): Internal extinction. Col. (4): The Galactic extinction. Col. (5): K-correction. Col. (6): E-correction. Col. (7): Corrected total magnitude without E-correction written by $m^0_{\rm T} \equiv m_{\rm T} - A_i - A_{\rm G} - K$. Col. (8): Corrected total magnitude written by $m^1_{\rm T} \equiv m_{\rm T} - A_i - A_{\rm G} - K - E$.

Table 4. Line-widths and total magnitudes.

Galaxy	cz km s^{-1}	i deg	$W_{\rm CO}$ km s^{-1}	$W^{\rm c}_{\rm CO}$ km s^{-1}	$W^{\rm c}_{\rm HI}$ km s^{-1}	$m^0_{\rm T}(J)$ mag	$m^1_{\rm T}(J)$ mag	$m^0_{\rm T}(H)$ mag	$m^1_{\rm T}(H)$ mag
IRAS 02185+0642	29347	33	356	654	581	13.85	13.95	13.17	13.27
I Zw 23	12224	49	104	138	189	12.74	12.79	12.24	12.28
CGCG 1113.7+2936	13880	58	248	293	306	13.37	13.42	12.31	12.36
IC 2846	12294	34	360	644	573	12.21	12.26	11.47	11.51
IRAS 14060+2919	35060	47	376	514	475	15.11	15.23	14.58	14.70
CGCG 1417.2+4759	21465	44	293	422	404	13.88	13.96	13.21	13.29
CGCG 1448.9+1654	13700	40	282	439	417	14.09	14.15	13.96	14.01
NGC 6007	10547	43	347	509	471	12.61	12.66	12.33	12.37
IRAS 16533+6216	31808	27	217	478	447	15.15	15.29	14.52	14.63
IRAS 23420+2227	26022	51	308	396	385	15.63	15.73	14.90	14.99

Col. (1): Galaxy name. Col. (2): Redshift in cz. Col. (3): Inclination. The inclination errors were measured to be about $4\overset{\circ}{.}8$ for all galaxies, and we adopted the same value through this paper. Col. (4): CO line-width. Col. (5): CO line-width corrected for the inclination. Col. (6): Converted CO line-width corresponding to H I line-width. Col. (7): Total magnitude defined as $m^0_{\rm T} \equiv m_{\rm T} - A_i - A_{\rm G} - K$ for J-band. Col. (8): Total magnitude defined as $m^1_{\rm T} \equiv m_{\rm T} - A_i - A_{\rm G} - K - E$ for J-band. Col. (9): $m^0_{\rm T}$ for H-band. Col. (8): $m^1_{\rm T}$ for H-band.

Table 5. Tully–Fisher distance and Hubble ratio.

Galaxy	cz	$D_{L\ K}$	$D_{L\ K,E}$	$H_{0\ K}$	$H_{0\ K,E}$
	$\mathrm{km\,s^{-1}}$	Mpc	Mpc	$\mathrm{km\,s^{-1}\,Mpc^{-1}}$	$\mathrm{km\,s^{-1}\,Mpc^{-1}}$
(J-band)					
PG 0157	48869	251 ± 37	271 ± 40	202 ± 30	187 ± 27
IR 02185	29347	421 ± 100	441 ± 105	71 ± 17	68 ± 16
IZw 23	12224	40 ± 6	40 ± 6	313 ± 49	306 ± 48
CG 1113	13880	118 ± 20	121 ± 21	118 ± 20	116 ± 20
IC 2846	12294	208 ± 50	213 ± 51	60 ± 14	58 ± 14
IR 14060	35060	562 ± 95	594 ± 100	64 ± 11	61 ± 10
CG 1417	21465	244 ± 44	253 ± 45	90 ± 16	86 ± 16
CG 1448	13700	284 ± 53	291 ± 55	49 ± 9	48 ± 9
N 6007	10547	177 ± 30	181 ± 30	60 ± 10	59 ± 10
IR 16533	31808	526 ± 156	561 ± 167	62 ± 18	58 ± 17
IR 23420	26022	493 ± 83	516 ± 87	54 ± 9	52 ± 9
(H-band)					
PG 0157	48869	235 ± 33	253 ± 36	216 ± 31	201 ± 28
IR 02185	29347	421 ± 97	441 ± 102	71 ± 16	68 ± 16
IZw 23	12224	50 ± 8	51 ± 8	245 ± 37	240 ± 37
CG 1113	13880	107 ± 18	110 ± 18	131 ± 22	128 ± 21
IC 2846	12294	189 ± 44	193 ± 45	66 ± 15	64 ± 15
IR 14060	35060	595 ± 98	629 ± 103	61 ± 10	57 ± 9
CG 1417	21465	260 ± 45	269 ± 47	84 ± 15	81 ± 14
CG 1448	13700	369 ± 67	378 ± 69	38 ± 7	37 ± 7
N 6007	10547	209 ± 34	213 ± 35	51 ± 8	50 ± 8
IR 16533	31808	530 ± 153	558 ± 161	62 ± 18	58 ± 17
IR 23420	26022	498 ± 81	519 ± 85	53 ± 9	51 ± 8

Col. (1): Galaxy name. Col. (2): Redshift in cz. Col. (3): Tully–Fisher distance corrected for K-correction. Col. (4): Tully–Fisher distance corrected for K- and E-corrections. Col. (5) and Col. (6): Hubble ratio for the Tully–Fisher distance in Col. (3) and Col. (4), respectively.

Table 6. Results of the CO-line Tully–Fisher relation.

Band	Correction	H_0
		$\mathrm{km\,s^{-1}\,Mpc^{-1}}$
J	K	60 ± 10
H	K	53 ± 13
J	$K + E$	58 ± 10
H	$K + E$	52 ± 12

Col. (1): Used band. Col. (2): Corrections applied to the total magnitude. K and E stand for K-correction and E-correction, respectively. Col. (3): Determined Hubble constants.

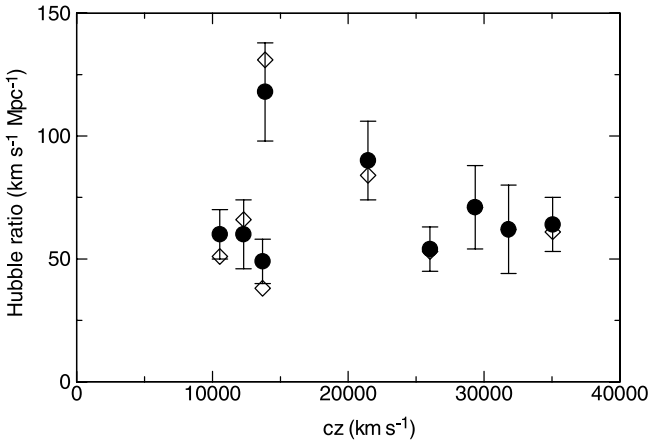

Fig. 3. Hubble ratios plotted against the redshifts for J- (filled circles) and H-band (diamonds), after a K-correction. Note the smaller scatter for redshifts larger than $\sim 20000\,\mathrm{km\,s^{-1}}$.

to obtain a more accurate Hubble constant, it is important to go to higher redshifts where the peculiar velocities are small compared to the recession velocity. On the other hand, the evolution effect becomes significant at higher redshifts, which is still not easy to correct for by the current models. These conflicting requirements can be optimized by applying the TFR to galaxies at intermediate redfhits. For such purposes, the CO TFR would potentially be an alternative to H I TFR, particularly when larger and more sensitive facilities, such as the ALMA, become available in the future.

We have thus shown that the CO TFR is quite possible for cosmological distances at $cz \sim 10000$–$50000\,\mathrm{km\,s^{-1}}$, although the detectability and the accuracy are not yet satisfactory. Nevertheless, we were able to determine the mean Hubble

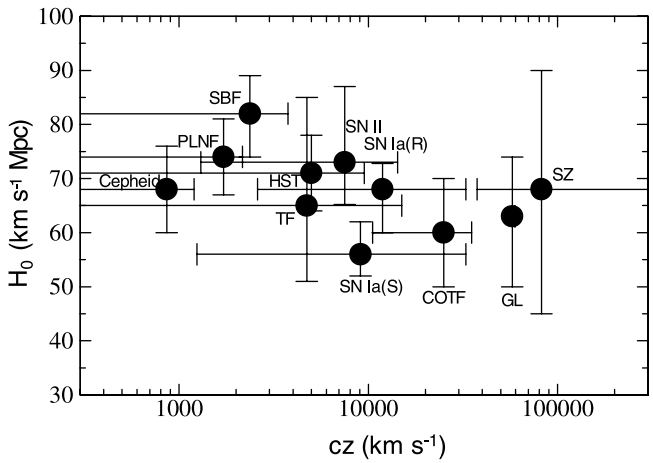

Fig. 4. Hubble constants determined by various methods (Okamura 1999). The references are: SBF (surface brightness fluctuation: Tonry 1991); PNLF (planetary nebulae luminosity function: Jacoby 1997); HST (The HST key project: Sakai et al. 2000); Cepheid (Tanvir et al. 1995); TF (Watanabe et al. 1998); SN II (Type II SN: Eastman et al. 1996); SN Ia(R) (Type Ia SN: Riess et al. 1995); SN Ia(S) (Type Ia SN: Sandage et al. 1996); GL (gravitational lens: Kundic et al. 1997); SZ (Sunyaev–Zel'dovich effect: Furuzawa et al. 1999); and COTF (This work).

constant in the space between $cz \sim 10000$ and $35000\,\mathrm{km\,s^{-1}}$ to be $H_0 = 60 \pm 10\,\mathrm{km\,s^{-1}\,Mpc^{-1}}$ from the J-band TFR.

Our value is consistent within the error with the recent value $H_0 = 65\,\mathrm{km\,s^{-1}\,Mpc^{-1}}$ from H I TFR at $cz < 12000\,\mathrm{km\,s^{-1}}$ (Watanabe et al. 1998), and is slightly smaller than that from the HST key project, $H_0 = 71\,\mathrm{km\,s^{-1}\,Mpc^{-1}}$, for galaxies within 25 Mpc and clusters within $10000\,\mathrm{km\,s^{-1}}$ (Mould et al. 2000). Our value is also consistent with those obtained at similar redshifts using Type I supernovae (Sakai et al. 2000; Branch 1998), those using the Sunyaev–Zel'dovich effect (Sunyaev, Zeldovich 1972; Hughes, Birkinshaw 1998), and those from gravitationally lensed QSOs (Williams, Saha 2000). In figure 4 we plot the recent values of Hubble constants derived from various methods, following Okamura (1999). The vertical bars indicate errors, and the horizontal bars the redshift coverage.

We emphasize that the present CO-line method provides an alternative, new tool to estimate the distances of intermediate-redshift galaxies within the scheme of the established Tully–Fisher relation. The thus-obtained Hubble constant can be directly compared with those obtained for nearer galaxies using the TFR.

We finally stress that the CO–NIR TFR will be a promising tool for high-redshift galaxies, which are supposed to be dusty, if the evolutionary effect can be properly corrected. The CO–NIR TFR, as proposed in this paper, will become one of the methods for cosmological distance estimates at high redshifts using the coming largest mm- and sub-mm-wave facility, ALMA, by which higher transition CO lines will be observed with much higher sensitivity. The present research using the 45-m telescope has been carried out in order to establish a methodology of the CO TFR, and to evaluate the feasibility for future projects using the Nobeyama mm-wave array and ALMA.

Y.T. and M.H. would like to thank the Japan Society for the Promotion of Science for the financial support for young researchers. IRAF is distributed by the National Optical Astronomy Observatories, which is operated by the Association of Universities for Research in Astronomy, Inc. (AURA) under a cooperative agreement with the National Science Foundation.

References

Aaronson, M., Huchra, J., & Mould, J. 1980, ApJ, 237, 655
Berstein, D., & Heiles, C. 1982, AJ, 87, 1165
Branch, D. 1998, ARA&A, 36, 17
Casoli, F., Boisse, P., Combes, F., & Dupraz, C. 1991, A&A, 249, 359
de Vaucouleurs, G., de Vaucouleurs, A., Corwin, H. G., Jr., Buta, R. J., Paturel, G., & Fouqué, P. 1991, Third Reference Catalogue of Bright Galaxies (RC3) (New York: Springer-Verlag)
Dickey, J. M., & Kazès, I. 1992, ApJ 393, 530
Eastman, R. G., Schmidt, B. P., & Kirshner, R. 1996, ApJ, 466, 911
Fisher, K. B., Huchra, J. P., Strauss, M. A., Davis, M., Yahil, A., & Schlegel, D. 1995, ApJS, 100, 69
Furuzawa, A., Tawara, Y., Yamashita, K., Miyoshi, S., & Matsuura, M. 1999, in Proceedings of IAU Symp. 183, Cosmological Parameters and the Evolution of the Universe, ed. K. Sato (Dordrecht: Kluwer), 66
Giovanelli, R., & Haynes, M. P. 1985, ApJ, 292, 404
Giovanelli, R., Haynes, M. P., Salzer, J. J., Wegner, G., Da Costa, L. N., Freudling, W. 1995, AJ, 110, 1059
Hamabe, M., & Ichikawa, S. 1992, in ASP Conf. Ser. 25, Proc. Astronomical Data Analysis Software and Systems I, ed. D. M. Worrall, C. Biemesderfer, & J. Barnes (San Francisco: Astronomical Society of the Pacific), 325
Haynes, M. P., & Giovanelli, R. 1986, ApJ, 306, 466
Hubble, E. 1926, ApJ, 64, 321
Hughes, J. P., & Birkinshaw, M. 1998, ApJ, 501, 1
Hunt, L. K., Mannucci, F., Testi, L., Migliorini, S., Stanga, R. M., Baffa, C., Lisi, F., & Vanzi, L. 1998, AJ, 115, 2594.
Jacoby, G. H. 1997, in The Extragalactic Distance Scale, ed. M. Livio, M. Donahue, & N. Panagia (Cambridge: Cambridge University Press), 197
Kenney, J. D., & Young, J. S. 1988, ApJS, 66, 261
Kundic, T., Turner, E. L., Colley, W. N., Gott, J. R., III, Rhoads, J. E., Wang, Y., Bergeron, L. E., Gloria, K. A., et al. 1997, ApJ, 482, 75
Lavezzi, T. E., & Dicky, J. M. 1998, AJ, 116, 2672
Mould, J. R., Huchra, J. P., Freedman, W. L., Kennicutt, R. C., Jr., Ferrarese, L., Ford, H. C., Gibson, B. K., Graham, J. A., et al. 2000, ApJ, 529, 786
Okamura, S. 1999, in Milky Way Galaxy and the Universe of Galaxies (Tokyo: University of Tokyo Press), 203 (in Japanese)
Poggianti, B. M. 1997, A&AS, 122, 399
Rieke, G. H., & Lebofsky, M. J. 1985, ApJ, 288, 618
Riess, A. G., Press, W. H., & Kirshner, R. P. 1995, ApJ, 438, L17
Sakai, S., Mould, J. R., Hughes, S. M. G., Huchra, J. P., Macri, L. M., Kennicutt, R. C., Jr., Gibson, B. K., Ferrarese, L., et al. 2000, ApJ, 529, 698
Sandage, A., Saha, A., Tammann, G. A., Labhardt, L., Panagia, N., & Macchetto, F. D. 1996, ApJ, 460, L15
Schöniger, F., & Sofue, Y. 1994, A&A 283, 21
Schöniger, F., & Sofue, Y. 1997, A&A 323, 14
Sofue, Y. 1992, PASJ, 44, L231

Sofue, Y., Schöniger, F., Honma, M., Tutui, Y., Ichikawa, T., Wakamatsu, K., Kazes, I., & Dickey, J. 1996, PASJ, 48, 657
Strauss, M. A., Huchra, J. P., Davis, M., Yahil, A., Fisher, K. B., & Tonry, J. 1992, ApJS, 83, 29
Sunyaev, R. A., & Zeldovich, Ya. B. 1972, in Comm. Astrophys. Space. Phys., 4, 173
Tanvir, N. R., Shanks, T., Ferguson, H. C., & Robinson, D. R. T. 1995, Nature, 377, 27
Tonry, J. L. 1991, ApJ, 373, L1
Tully, R. B., & Fisher, J. R. 1977, A&A, 54, 661
Tutui, Y., & Sofue, Y. 1999, A&A, 351, 467
Tutui, Y. 1999, Ph.D. Thesis, The University of Tokyo
Tutui, Y., Sofue, Y., Honma, M., Ichikawa, T., & Wakamatsu, K. 2000, PASJ, 52, 803.
van Driel, W., van den Broek, A. C., & Baan, W. A. 1995, ApJ, 444, 80
Watanabe, M., Ichikawa, T., & Okamura, S. 1998, ApJ, 503, 553
Watanabe, M., Yasuda, N., Itoh, N., Ichikawa, T., & Yanagisawa, K. 2001, ApJ, 555, 215
Williams, L. L. R., & Saha, P. 2000, AJ, 119, 439